Urmia University

Water and Environmental Challenges

2025;1(1):50-61

Journal homepage: https://jwec.urmia.ac.ir

Water & Environmental Challenges

Analysis of the Risk of Late Spring Frosts using Satellite Remote Sensing Products in West Azerbaijan Province

Somayeh Hejabi [a*], Esmaeil Simaei [b], Azad Tohidi [c], Hamideh Motiei [d]

[a] Associate Professor, Department of Water Engineering, Urmia University, Urmia, Iran
[b] General Director of Administration of Meteorology of West Azerbaijan Province, Urmia, Iran
[c] Head of Applied Meteorology Research Group of West Azerbaijan Meteorology, Urmia, Iran
[d] Weather Forecaster, Administration of Meteorology of West Azerbaijan Province, Urmia, Iran

A B S T R A C T

This study investigates the risk of late spring frosts in West Azerbaijan province by developing a minimum air temperature estimation model. Utilizing daily minimum air temperature data from 20 meteorological stations, satellite-derived land surface temperature, and auxiliary data, a statistical model was developed. Subsequently, daily minimum temperature maps for potential spring frost months (in the period 2000-2023) were generated to analyze late spring frost risk. This research provides two novel tools: a code to estimate frost occurrence risk for specific day numbers and temperature thresholds, and another code to estimate the day number corresponding to a given risk percentage and temperature threshold. The frost risk estimation code offers 17,690 possible scenarios, while the day number estimation code provides 2,755, enabling detailed frost risk analysis for various plant sensitivities and optimized planting date determination. The resulting frost risk maps are valuable for determining suitable crop cultivation times and locations, considering varying plant sensitivity thresholds to frost.

Keywords:
Frost Risk Map
Land Surface Temperature
Minimum Air Temperature Model
MODIS Product

1. Introduction

Frost is defined as a condition where the air temperature near the Earth's surface drops below zero degrees Celsius. Freezing occurs when the air temperature in a large area remains below zero degrees Celsius for a sufficient period of time (at least 1 or 2 days) (Huschke, 1959). However, agricultural meteorologists believe that agricultural frosts begin at a higher threshold, often considering +4 degrees Celsius as the starting point for frost damage to plant tissues (Bazrafshan and Rahimi, 2014). Although plants are highly resistant to sub-freezing temperatures during winter dormancy, during active growth, the sensitive tissues of plants, including new buds, leaves, and flowers, are vulnerable to frost (Inouye, 2000). Freezing can cause damage to plants, and the severity of the damage depends on the intensity and duration of the frost. When a plant freezes, ice forms inside or outside the cells. Intracellular freezing is immediately destructive, while extracellular freezing can cause varying levels of damage depending on the rate and extent of the dehydration process (Weiser et al., 1979). Chilling injury occurs when physiological damage is caused to the plant in the temperature range of 0 to +10 degrees Celsius.

* Corresponding authors.
E-mail address: s.hejabi@urmia.ac.ir
https://doi.org/10.30466/jwec.2025.56032.1006
Received: 18 June 2024
Accepted: 28 October 2024

The terms chilling injury and frost are often used interchangeably. Generally, there are two types of agricultural damage caused by frost. The first type is damage caused by unusually low winter temperatures over a long period, and the second type is damage caused by damaging sub-zero temperatures that occur as rare and short-term events (Kalma et al., 1992). The severity of frost damage depends on the phenological stage of plant development relative to the occurrence of low temperatures. Since both the occurrence of frosts and plant phenology are related to seasonal temperature changes, both are subject to climate change conditions. Therefore, in the future, the risk of frost damage will depend not only on changes in the frequency and occurrence of frost days but also on the shift in plant phenology (Lamichhane, 2021).

Frosts are usually categorized as advective, radiative, or a combination of these two types. Advective (dynamic) frosts occur as a result of the intrusion of a large-scale cold air mass from polar regions and develop during the day or night. This type of frost is characterized by moderate to strong winds and turbulent atmosphere and can become a problem for agriculture in high latitude or high altitude areas. Radiative frosts occur at night and are caused by intense long-wave radiation cooling under calm, clear, and dry atmospheric conditions. Under these conditions, strong inversions develop in the stable atmosphere (Kalma et al., 1992).

In another classification, frosts are categorized based on their time of occurrence into winter frosts, early autumn frosts (EAFs), and late spring frosts (LSFs). Winter frosts (such as the near-nationwide cold wave in the winter of 2008) at a certain temperature threshold can cause significant damage to fruit trees, especially citrus, pomegranates, and vineyards, to the point of complete destruction (Khalili, 2014). The study of early autumn and late spring frosts is important because many agricultural activities, including the cultivation of autumn wheat and barley, coincide with early autumn frosts, and the flowering of fruit trees coincides with late spring frosts (Aghashariatmadari et al., 2016).

Late spring frosts have significant ecological and economic impacts on agriculture and forestry. Damage caused by late spring frosts to vulnerable plant organs significantly affects growth, health, interspecific competition, carbon sequestration, and plant distribution ranges (Lamichhane, 2021). The spring frost that occurred in April 2007 in the south-central and southeastern United States caused agricultural losses of approximately 1.6 billion euros (Marino et al., 2011). The economic losses caused by the April 2017 frost in Central and Western Europe were estimated at over 80 million euros for fruit crops in Switzerland and 3.3 billion euros for all affected European regions (Vitasse and Rebetez, 2018). In Iran, a large percentage of the compensation paid to farmers by the Agricultural Products Insurance Fund annually relates to frost and freezing damage. According to the statistics of the Comprehensive Agricultural Insurance System (SABKA, 2023), feezing and frost are the second most damaging factors to insured agricultural products, after drought. West Azerbaijan province, with over 800,000 hectares of orchards and farmlands, is one of the successful provinces in agriculture, producing 6.8 million tons of various agricultural products annually, worth 33 trillion Tomans, with an added-value of 17.8%. Due to the region's climate and the lack of necessary facilities for modern frost control methods for most farmers, it is threatened by freezing and frost damage every year. In the spring of 2023, the West Azerbaijan Agricultural Jihad Organization reported damage to about 30% of orchards due to frost, estimating spring frost damage to about 50,000 tons of products from 21,000 hectares of orchards in the province.

One of the essential requirements for reducing frost damage is frost risk management. Also, the Agricultural Products Insurance Fund, which is legally responsible for implementing management policies in the agricultural sector, needs to quantify the risk of frost occurrence in different parts of the country to fairly assess frost risk and make data-driven decisions in insuring agricultural products against frost events (Khalili, 2014). The frequency and intensity of frosts, as well as the duration of the frost season, are among the most important factors determining the possibility of crop cultivation in an agricultural area. Long-term weather data can provide a good indicator of frost risk, i.e., the probability of a certain sub-zero temperature occurring at a specific time. Therefore, frost risk maps are important tools for land use planning and farm and crop management in agriculture and horticulture. These maps are also essential for local interpretation or short-term frost forecasts at the regional scale and for frost control technologies (Kalma et al., 1992).

The first attempts to study frost in Iran date back to the 1970s. According to Khalili (2014), Hashemi (1974) studied the dates of occurrence of early autumn and late spring frosts with a scale accuracy of 1:16,000,000 for the network of synoptic stations in Iran, and prepared a map of the length of the growing season and active growth days based on statistics from 1961 to 1970. The second effort to study the occurrence of damaging frosts was Kamali (2001), in which the dates of crossing the first and last specific temperatures at probability levels of 25, 50, and 75 percent were examined, and isochronous lines were drawn based on linear interpolation with temperature estimation at multiple altitude points in the country. Also, Khalili (2009) aimed at zoning frost risk at different phenological stages of various crops, provided maps of the dates of occurrence of early autumn frost, late spring frost, and the duration of frost for various thresholds of damaging temperatures at different probability levels from 10 to 90 percent in a GIS environment with an accuracy of 1×1 kilometer for the extent of Iran as a climatic atlas.

Maps of meteorological components (e.g., minimum air temperature or the probability of frost occurrence) are generally based on a network of meteorological stations. However, especially in areas with complex topography, the density of the meteorological station network is rarely sufficient. Many of the techniques used by researchers to generate spatial distribution patterns of meteorological components are based on fitting multidimensional smooth spline functions and spatial analysis and interpolation methods, such as Kriging, Co-Kriging, and Inverse Distance Weighting. However, interpolation errors, depending on the temporal and spatial scale and the technique used, are generally between 1 and 3 degrees Celsius (Mostovoy et al., 2006). Hesari et al. (2015) analyzed the probabilistic occurrence of frost based on the minimum temperature statistics of 34 synoptic and evaporation measurement stations in West Azerbaijan province and prepared a map of the frost occurrence date at a 75 percent probability using Kriging, Co-Kriging, and Inverse Distance Weighting methods. Considering the complex topography of the province, the insufficient density of stations, the concentration of stations at low altitudes, as well as the dependence of minimum temperature and frost intensity on other factors such as land use type, plant phenological development, soil moisture, distance from water bodies, daily solar radiation cycle, solar zenith angle, etc., the use of spatial interpolation methods is not sufficient to prepare frost risk maps. Therefore, the use of more accurate methods that consider a significant portion of the aforementioned factors is necessary in preparing more accurate temperature and frost risk maps.

One of the methods for mapping frost-prone areas is the use of three-dimensional numerical models that simulate the surface microclimate of heterogeneous areas during radiative frost events and can be used to generate minimum air temperature maps. These models are based on solving the physical equations of energy balance for the soil surface and vegetation canopy and can consider the effects of soil and vegetation on latent and sensible heat fluxes, and consequently, on air temperature and ground surface temperature.

Another method is a semi-empirical approach to assess spatial patterns of frost risk at a regional scale, considering meteorological data and land surface data. In the simplest case, a model can be a regression relationship between minimum air temperature and altitude. However, extrapolating temperature to altitude ranges outside the range of altitudes of the stations used for model calibration can carry significant risk. Additionally, Kalma et al. (1986) showed that near-surface air temperature is strongly dependent on land cover. Therefore, maps derived from empirical methods should only be used for land covers similar to those where the data were obtained and the model was calibrated.

In recent years, remote sensing technology has been widely used in frost risk zoning and frost forecasting. Thermal radiation sensing in the 8-14 μm wavelength band, a range where radiation absorption by water vapor is minimal, can help assess land surface temperature (LST) by measuring radiation. Many researchers have presented methods for estimating air temperature using remote sensing data. Although LST and air temperature are strongly correlated, they differ in physical meaning, values, measurement techniques, and diurnal phase, and have different responses to atmospheric conditions (Jin and Dickinson, 2010). Mildrexler et al. (2011) showed that altitude, topography, and surface roughness are important in the relationship between LST and air temperature. Jin and Dickinson (2010) also demonstrated the importance of cloud cover, water vapor content, and vegetation cover on the land-atmosphere system. A common method for estimating air temperature based on LST is to use statistical approaches based on univariate or multivariate regression techniques (e.g., Mostovoy et al., 2006; Jang et al., 2004). These methods are based on data measured at meteorological stations as predictor variables, and it is assumed that the measured dataset is a subset of the overall air temperature distribution and therefore contains information about the reality of the spatial distribution of air temperature in a large area. Therefore, the use of statistical methods based on predictors such as LST data from satellite remote sensing products and auxiliary data (e.g., altitude, distance from water bodies, latitude, longitude, etc.) can be considered an effective approach in estimating minimum air temperature and preparing gridded minimum temperature data for frost risk analysis.

Benali et al. (2012) used a statistical method based on LST data and auxiliary data to estimate minimum temperature, maximum temperature, and mean air temperature over a 10-year period. The efficiency index of the presented model was 0.941 for mean air temperature and 0.871 and 0.919 for minimum and maximum temperatures, respectively, and could provide weekly temperature estimates at a 1 km spatial scale, accurately describing intra-annual and inter-annual temporal and spatial patterns of air temperature. A valuable study on estimating air temperature based on LST data in Iran is the study by Janatian et al. (2016), who presented an advanced statistical approach for estimating air temperature over a 5-year period in eastern Iran based on LST data and 11 auxiliary data, and showed that the presented model had a mean absolute error of 2.3 and 1.8 degrees Celsius at daily and weekly scales, respectively.

So far, no study has been conducted on estimating air temperature based on remote sensing data in West Azerbaijan province, and frost risk analysis studies (such as Hesari et al., 2015; Bazgir et al., 2016) have been based on limited station data. Given the large temporal and spatial variations in air temperature, the influence of various factors on air temperature, and the importance of remote sensing data in terms of having suitable temporal and spatial resolutions, it is necessary to prepare gridded air temperature data with a suitable spatial scale for more accurate frost risk analysis. The main objective of this study is to analyze the risk of late spring frosts in West Azerbaijan province. In this regard, the sub-objectives of this study are as follows:

1. To present a statistical model based on satellite remote sensing products to estimate minimum air temperature.
2. To prepare gridded minimum air temperature data based on the developed model.
3. To probabilistically analyze late spring frosts based on gridded minimum air temperature data and to present frost risk maps.

2. Materials and Methods

2.1. Study Area

The study area is the province of West Azerbaijan. West Azerbaijan province is located in northwestern Iran and is bordered by the Republic of Azerbaijan and Turkey to the north, Turkey and Iraq to the west, East Azerbaijan province and Zanjan province to the east, and Kurdistan province to the south. The area of the province is 37,059 square kilometers, making it the thirteenth largest province in the country and comprising 2.25% of the total area of the country. Figure 1 shows the geographical location of West Azerbaijan province.

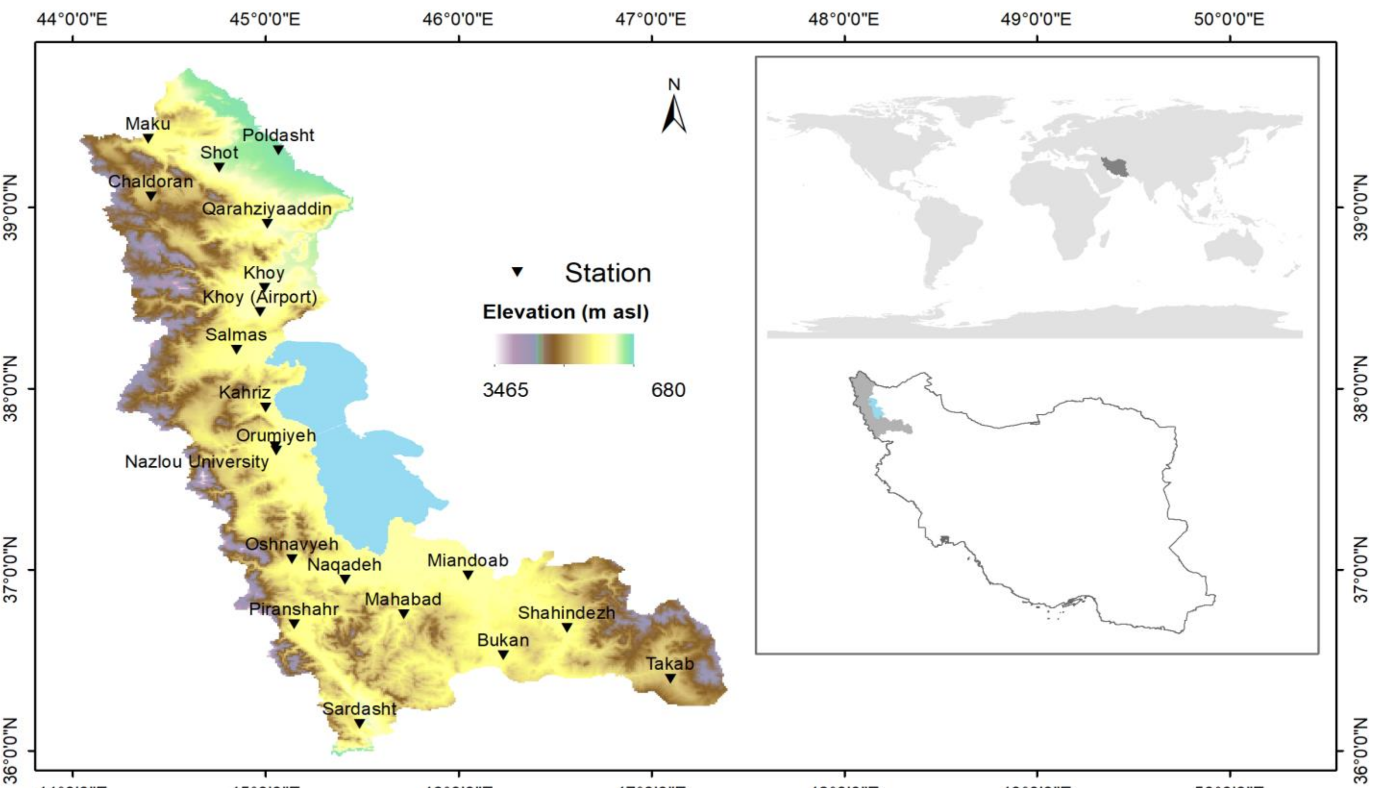

Figure 1. Geographical location of West Azerbaijan province and the studied meteorological stations. The inset shows the location of West Azerbaijan province in the national and global contexts

2.2. Data

The first phase of the study includes the preparation of minimum air temperature data from meteorological stations and land surface temperature (LST) data from satellite remote sensing products to complete the predictor and predictand datasets. Accordingly, the steps of the first phase are as follows:

1. Preparation of minimum air temperature data from meteorological stations: The meteorological stations in the West Azerbaijan province include 20 stations, and the minimum air temperature data of these stations were obtained from the administration of Meteorology of West Azerbaijan Province. The location of the studied stations is shown in Figure 1. Information such as altitude, latitude, and longitude will be used as predictor variables for minimum air temperature.
2. Preparation of gridded altitude data: Since gridded altitude data are needed to prepare minimum air temperature maps, the global data of the SRTM (Shuttle Radar Topography Mission,

2013) digital elevation model with a spatial resolution of 30 meters were applied. To check the accuracy of these data, the altitude of the cells corresponding to the coordinates of each station was extracted using ArcGIS software. Comparing the altitude of the stations with their corresponding values from SRTM data indicates their high correlation (r = 0.999).

3. Calculation of solar zenith angle: Considering the relationship between temperature changes and the daily cycle of solar radiation, examining the solar zenith angle as another predictor variable of minimum air temperature is important. Based on latitude and altitude information of the stations, through coding in the MATLAB environment, the solar zenith angle was calculated daily for the statistical period of each station. Using the mentioned code and based on the altitude and latitude information of the SRTM grid cells, solar zenith angle maps for the studied statistical period can be prepared.

4. Calculation of the distance of stations from water bodies: Considering that the weather conditions in an area can be affected by the distance from water bodies, the distance of each station from the coast of Lake Urmia was calculated using ArcGIS software. Similarly, the distance of each SRTM grid cell from the coast of Lake Urmia can also be calculated.

5. Preparation of land surface temperature (LST) data from satellite remote sensing products: As another predictor variable of minimum air temperature, version 6.1 of the MOD11A1 land surface temperature (LST) product from the Moderate Resolution Imaging Spectroradiometer (MODIS) sensor on the Terra satellite is used. These data have a daily temporal scale and a spatial resolution of 1 km and are available for day and night for the statistical period of 24/2/2000 onwards. In the first step, through coding in the Google Earth Engine environment, the night LST values of the available statistical period were extracted for the cells corresponding to each of the synoptic stations, and based on the data quality control information in the MOD11A1 product metadata, data with high errors were removed.

2.3. Development of the Minimum Temperature Estimation Model

The second phase of the study involves data analysis, the development of a minimum temperature estimation model, and the preparation of gridded minimum air temperature data based on the developed model. For this purpose, the predictand data (minimum air temperature (Tmin) at the studied stations) and predictor data (including land surface temperature (LST) data, Julian day number (JD), solar zenith angle (Z), station altitude (ELV), station longitude (LON) and latitude (LAT), land slope at the station (SLP), land aspect at the station (ASP), and the station's distance from coast of Lake Urmia (D2C)) prepared in the first phase were integrated into series, and days with statistical gaps in minimum temperature or land surface temperature were removed. The relationship between temperature and day number follows the trigonometric relationship below:

$$F(JD)=\cos\left[\frac{2\pi(JD-JD_{peak})}{365}\right] \quad (1)$$

Where JD is the Julian day number and JD_{peak} is the Julian day number corresponding to the warmest day of the year, which is considered here to be 218 (August 6th). Using equation (1), the function value for different values of the Julian day number (F(JD)) was calculated and used as a model input variable. Also, the minimum temperature is correlated to the cosine of the solar zenith angle (cos(Z)) and the sine of half the aspect (sin(ASP/2)). For land surface temperature and solar zenith angle, data from the previous day (t-1) were used to predict the minimum temperature on day t. First, to determine the variables that show a significant correlation with the minimum temperature, a cross-correlation matrix between the predictor and predictand variables was prepared. Then, regression analysis was performed in Minitab software using a stepwise method and with random division of the data into calibration and test data with a ratio of 70% and 30%. Finally, based on the statistical criteria of the coefficient of determination (R^2), root mean square error (RMSE), and mean absolute error (MAE), the most suitable minimum temperature estimation model was selected.

$$R^2 = \left(\frac{\sum_{i=1}^{n}(X_{OBS_i}-\bar{X}_{OBS})(X_{MODEL_i}-\bar{X}_{MODEL})}{\sqrt{\sum_{i=1}^{n}(X_{OBS_i}-\bar{X}_{OBS})^2(X_{MODEL_i}-\bar{X}_{MODEL})^2}}\right)^2 \quad (2)$$

$$RMSE = \sqrt{\frac{\sum_{i=1}^{n}(X_{MODEL_i}-X_{OBS_i})^2}{n}} \quad (3)$$

$$MAE = \frac{\sum_{i=1}^{n}|X_{MODEL_i}-X_{OBS_i}|}{n} \quad (4)$$

Where $\bar{X}$ is the mean of variable X (minimum temperature) and the subscripts MODEL and OBS represent the modeled and observed values, respectively. After determining the selected model, simulated minimum temperature maps were prepared daily in the Google Earth Engine environment using the selected model for the statistical period of 2000-2023 with a spatial resolution of 1 kilometer and in .tif format.

2.4. Analysis of Late Spring Frost Risk

In the final phase of the study, using the daily minimum temperature maps for the months of March, April, May, and June for the statistical period of 2000-2023, the risk analysis of late spring frosts was performed. For this purpose, through coding in the MATLAB software environment, the minimum temperature maps in .tif format were called, and for each map pixel (with dimensions of 1 km × 1 km), the daily minimum temperature data for the months of March, April, May, and June for the statistical period of 2000-2023 were extracted, and for a specific temperature threshold for frost occurrence, the day number corresponding to the last late spring frost for each year was determined. Examining the obtained time series showed that the Generalized Extreme Value (GEV) probability distribution fits the time series well. Therefore, by fitting the GEV probability distribution to the time series of the day number of the last late spring frost, for each pixel, the three parameters related to the GEV distribution were estimated in the MATLAB software environment. In the next step, the fitted probability distributions for each pixel were used to calculate the cumulative probabilities (p) of the day numbers corresponding to March 1st to June 30th (day numbers 152 to 273 with the origin of Mehr 1st [September 23rd]). The values of 1-p represent the risk of late spring frost occurrence on day d and thereafter. The MATLAB code was executed for different temperature thresholds of frost occurrence, including -10°C to +4.4°C with 0.1°C intervals (145 thresholds), and for each run, an Excel file containing the values of 1-p (risk) for day numbers 152 to 273 for different pixels was generated. The 145 generated Excel files were called in the Python programming environment, and using the commands of the Arcpy package, a shapefile was generated for each Excel file, whose descriptive information table contains the values of 1-p (frost occurrence risk) for day numbers 152 to 273 for different pixels at the corresponding temperature threshold. In the next step, another code named FrostRisk_code.py was written in the Python environment, which allows the user to generate a late spring frost risk map for a desired temperature threshold and day number by entering a desired temperature threshold (Tr) in the range of -10°C to +4.4°C and a desired day number (day). The generated map, named prob_Tr_day, is a raster layer with a spatial resolution of 1 km, and the value of each pixel represents the probability of late spring frost occurrence on a desired day for the frost occurrence temperature threshold (Tr). In addition, this code has the ability to generate the risk value point-wisely for any number of desired points as an Excel file. For this purpose, an input Excel file named point.xls containing the longitude and latitude of the points for which the risk value needs to be extracted should be prepared. The Python code calls this Excel file and, in addition to preparing the risk map, stores the late spring frost occurrence risk value for the desired points in an output Excel file named results_Tr_day.xls. Therefore, the output of the Python code is a raster layer and an Excel file that are stored in a folder named Outputs.

Another important issue in late spring frost analysis is knowing on what day the late spring frost occurs for a given temperature threshold (Tr) and a given risk (1-p). For this purpose, based on the estimated parameters of the GEV distribution in the previous step, a code was written in the MATLAB software environment that calculates the day number corresponding to the respective probability for different probabilities (risks) of 5 to 95 percent (with 5 percent intervals) for each specific temperature threshold. This code was executed for different temperature thresholds of frost occurrence, including -10°C to +4.4°C with 0.1°C intervals (145 thresholds), and for each run, an Excel file containing the day number of frost occurrence for risks of 5 percent to 95 percent for different pixels was generated. The 145 generated Excel files were called in the Python programming environment, and using the commands of the Arcpy package, a shapefile was generated for each Excel file, whose descriptive information table contains the day number for risks of 5 percent to 95 percent for different pixels at the corresponding temperature threshold. In the next step, another code named FrostDay_code.py was written in the Python environment, which allows the user to generate a late spring frost occurrence day number map for a desired temperature threshold and risk percentage by entering a desired temperature threshold (Tr) in the range of -10°C to +4.4°C and a desired risk percentage (risk). The generated map, named dy_Tr_risk, is a raster layer with a spatial resolution of 1 km, and the value of each pixel represents the day number of late spring frost occurrence for the risk (risk) and frost occurrence temperature threshold (Tr). In addition, this code has the ability to generate the day number of frost occurrence point-wisely for any number of desired points as an Excel file. For this purpose, an input Excel file named point.xls containing the longitude and latitude of the points for which the day number of frost occurrence needs to be extracted should be prepared. The Python code calls this Excel file and, in addition to preparing the frost occurrence day number map, stores the late spring frost occurrence day number value for the desired points in an output Excel file named results_Tr_risk.xls. Therefore, the output of the Python code is a raster layer and an Excel file that are stored in a folder named Outputs.

3. Results and discussion

3.1. Selection of the Minimum Temperature Estimation Model

To determine the variables that show a significant correlation with the minimum temperature, a cross-correlation matrix between the predictor and predictand variables was prepared. Table (1) shows the cross-correlation matrix of the studied variables.

Table 1. Cross-correlation matrix of the studied variables

	Tmin	LST	cos(Z)	F(JD)	ELV	LON	LAT	sin(ASP/2)	SLP
LST	0.949*								
cos(Z)	0.757*	0.782*							
F(JD)	0.854*	0.890*	0.655*						
ELV	-0.132*	-0.134*	0.010	-0.019*					
LON	-0.010	0.050*	0.078*	0.023*	0.268*				
LAT	-0.004	-0.039*	-0.059*	0.013*	-0.328*	-0.780*			
sin(ASP/2)	-0.063*	-0.11*	-0.051*	-0.038*	0.062*	-0.278*	0.373*		
SLP	0.070*	-0.010	0.005	-0.010	0.421*	0.063*	-0.213*	-0.017*	
D2C	-0.003*	-0.027*	0.031*	0.026*	0.433*	0.255*	0.106*	0.126*	0.462*

According to Table (1), the minimum temperature shows a positive and significant correlation (α=0.05) with LST. The variables F(JD) and cos(Z) are in the next positions in terms of correlation. The correlation of minimum temperature with altitude is negative and significant, but the minimum temperature does not show a significant correlation with longitude and latitude. Therefore, these two variables were not used in the model. The minimum temperature shows a weak positive and significant correlation with slope. Since steeper slopes receive less energy from the sun, it is expected that the correlation of temperature with slope would be negative. Since slope variations in the region are large and the existing stations cannot show a correct representation of slope variations and their relationship with temperature, the slope variable was not used in the regression analysis. Regarding aspect, it is expected that the relationship between temperature and sin(ASP/2) would be positive, but according to Table (1), the correlation is negative. Therefore, this variable was also not used in the regression analysis. Despite the weak correlation of minimum temperature with distance from water bodies, it was used in the regression analysis because of its significance.

Regression analysis was performed in Minitab software using a stepwise method and with random division of the data into calibration and test data with a ratio of 70% and 30%. Table (2) shows the regression coefficients of different combinations of input variables in different regression models.

Table 2. Regression coefficients of different regression models

n	Model	a	b	c	d	e	f
1	Tmin=a+b*LST	0.69	0.85				
2	Tmin=a+b*F(JDS)	6.05	10.89				
3	Tmin=a+b*LST+c*cos(Z)	-0.60	0.82	1.981			
4	Tmin=a+b*LST+c*D2C	0.42	0.85	4.00E-06			
5	Tmin=a+b*LST+c*cos(Z)+d*F(JD)	-0.50	0.78	2.257	0.684		
6	Tmin=a+b*LST+c*cos(Z)+d*D2C	-0.76	0.83	1.845	4.00E-06		
7	Tmin=a+b*LST+c*cos(Z)+d*F(JD)+e*D2C	-0.65	0.78	2.116	0.623	3.00E-06	
8	Tmin=a+b*LST+c*cos(Z)+d*F(JD)+e*ELV	0.34	0.76	2.590	0.817	-7.26E-04	
9	Tmin=a+b*LST+c*cos(Z)+d*F(JD)+e*ELV+f*D2C	0.66	0.76	2.570	0.802	-1.21E-03	6.00E-06

According to Table (2), the sign of the regression coefficient of the distance from water bodies (D2C) variable is positive, while according to Table (1), the correlation between minimum temperature and D2C is negative. Statistically, when the correlation coefficient and the regression coefficient of two variables have different signs, the relationship between these two variables is meaningless (Falk and Miller, 1992). This happens when the correlations, despite being significant, are very weak and close to zero. Therefore, models 4, 6, 7, and 9 were discarded. The criteria for evaluating the performance of other models are shown in Table (3).

Table 3. Criteria for evaluating regression models

n	Model	R^2	R^2 (adj)	Test R^2	RMSE	Test RMSE	MAE	Test MAE
1	Tmin=a+b*LST	0.900	0.900	0.899	2.728	2.741	2.069	2.081
2	Tmin=a+b*F(JDS)	0.729	0.729	0.730	4.501	4.477	3.532	3.524
3	Tmin=a+b*LST+c*cos(Z)	0.901	0.901	0.899	2.720	2.733	2.066	2.080
5	Tmin=a+b*LST+c*cos(Z)+d*F(JD)	0.902	0.902	0.900	2.712	2.722	2.071	2.082
8	Tmin=a+b*LST+c*cos(Z)+d*F(JD)+e*ELV	0.902	0.902	0.900	2.708	2.720	2.069	2.083

According to Table (3), model 2 has a significant performance difference compared to the other models. The best performance, with a slight difference from the other models, belongs to model 8. However, model 1, with fewer inputs and accuracy very close to model 8, was selected as the final model for estimating the minimum temperature for the statistical period of 2000 to 2023. Figure (2) shows the results of simulating the minimum temperature at the level of West Azerbaijan province, by applying model 1 to the gridded LST data, for example, on four dates in different seasons of 2022.

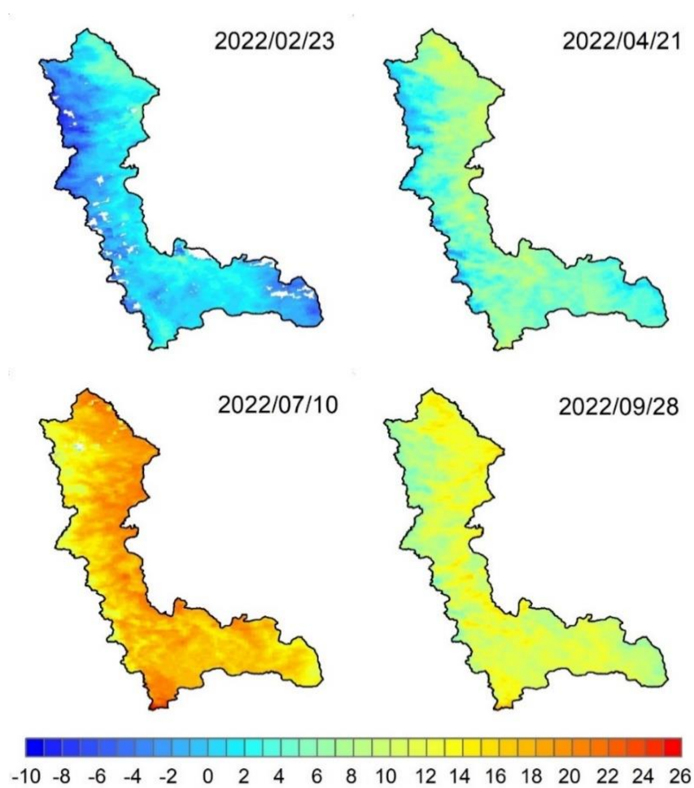

Figure 2. Results of minimum temperature simulation using model 1 on four dates in different seasons of 2022

3.2. Analysis of Late Spring Frost Risk

The analysis of spring frost risk can be performed in two ways using the FrostRisk_code.py and FrostDay_code.py codes. The FrostRisk_code.py code generates a frost occurrence risk map on a desired day and thereafter for a desired frost occurrence temperature threshold (Tr) and desired day number (day). Additionally, by entering longitude and latitude information of desired points in the input Excel file point.xls, it stores the frost occurrence risk values on day 'day' and thereafter for the threshold Tr for the desired points in an output Excel file named results_Tr_day.xls. The results of running the code for temperature thresholds of +4.4°C, 0°C, and -4.4°C on April 4th (185), April 21st (202), May 5th (216), and May 22nd (233) are shown in Figure (3). According to Figure (3), the probability of late spring frost occurrence decreases with increasing day number and decreasing temperature threshold.

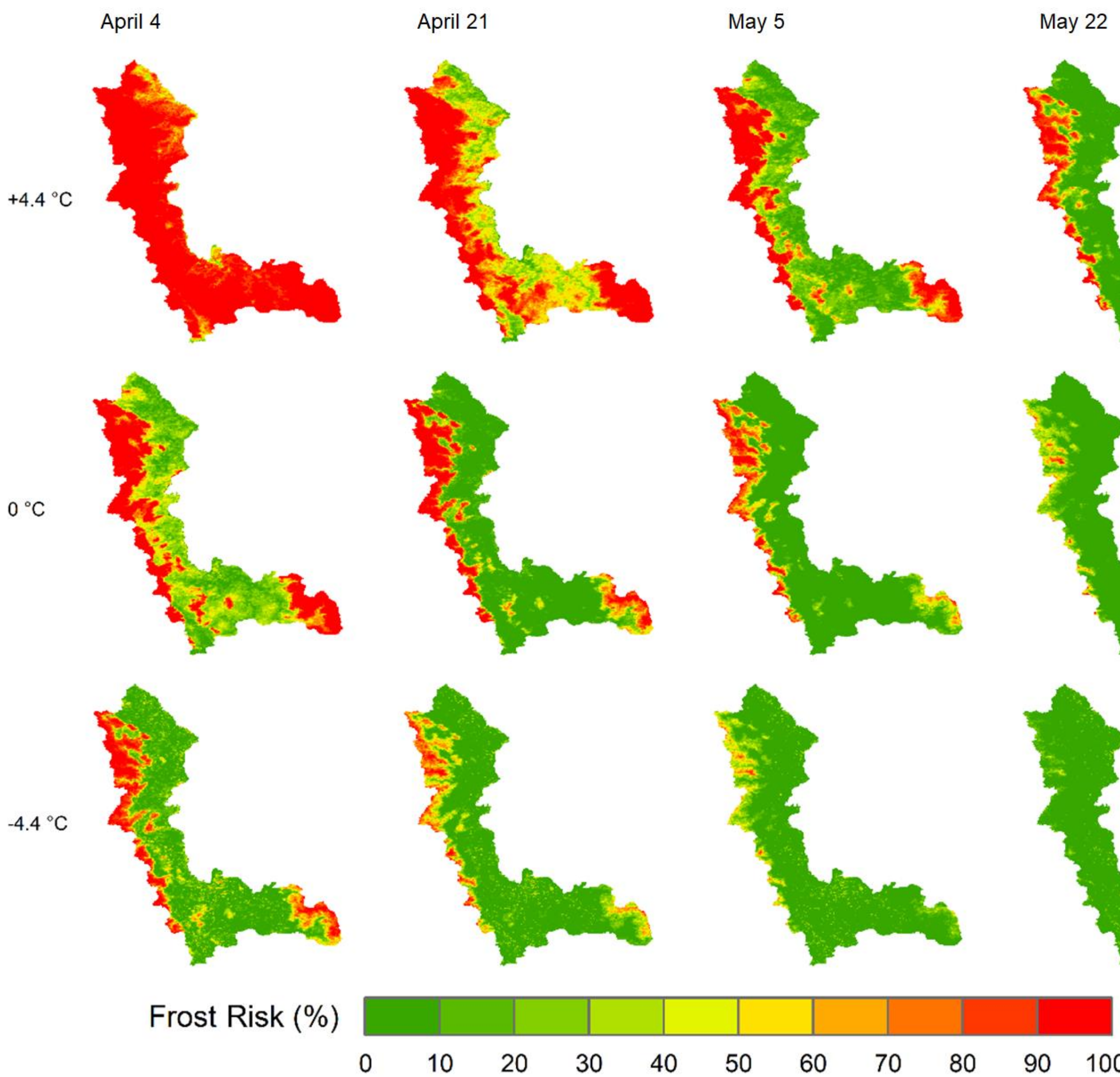

Figure 3. Frost occurrence risk maps for temperature thresholds of +4.4°C, 0°C, and -4.4°C on April 4th, April 21st, May 5th, and May 22nd.

The FrostDay_code.py code generates a frost occurrence day number map for a desired risk for a desired frost occurrence temperature threshold (Tr) and desired risk percentage (risk). Additionally, by entering longitude and latitude information of desired points in the input Excel file point.xls, it stores the frost occurrence day number values for the given risk (risk) for the threshold Tr for the desired points in an output Excel file named results_Tr_risk.xls. The results of running the code for temperature thresholds of +4.4°C, 0°C, and -4.4°C and risks of 5%, 25%, 50%, and 75% are shown in Figure (4). According to Figure (4), the day number of late spring frost occurrence decreases with increasing risk and decreasing temperature threshold.

The black pixels in Figure (4) represent points where, for the given temperature threshold and/or risk, frost does not occur on any day after day 150 (February 27th).

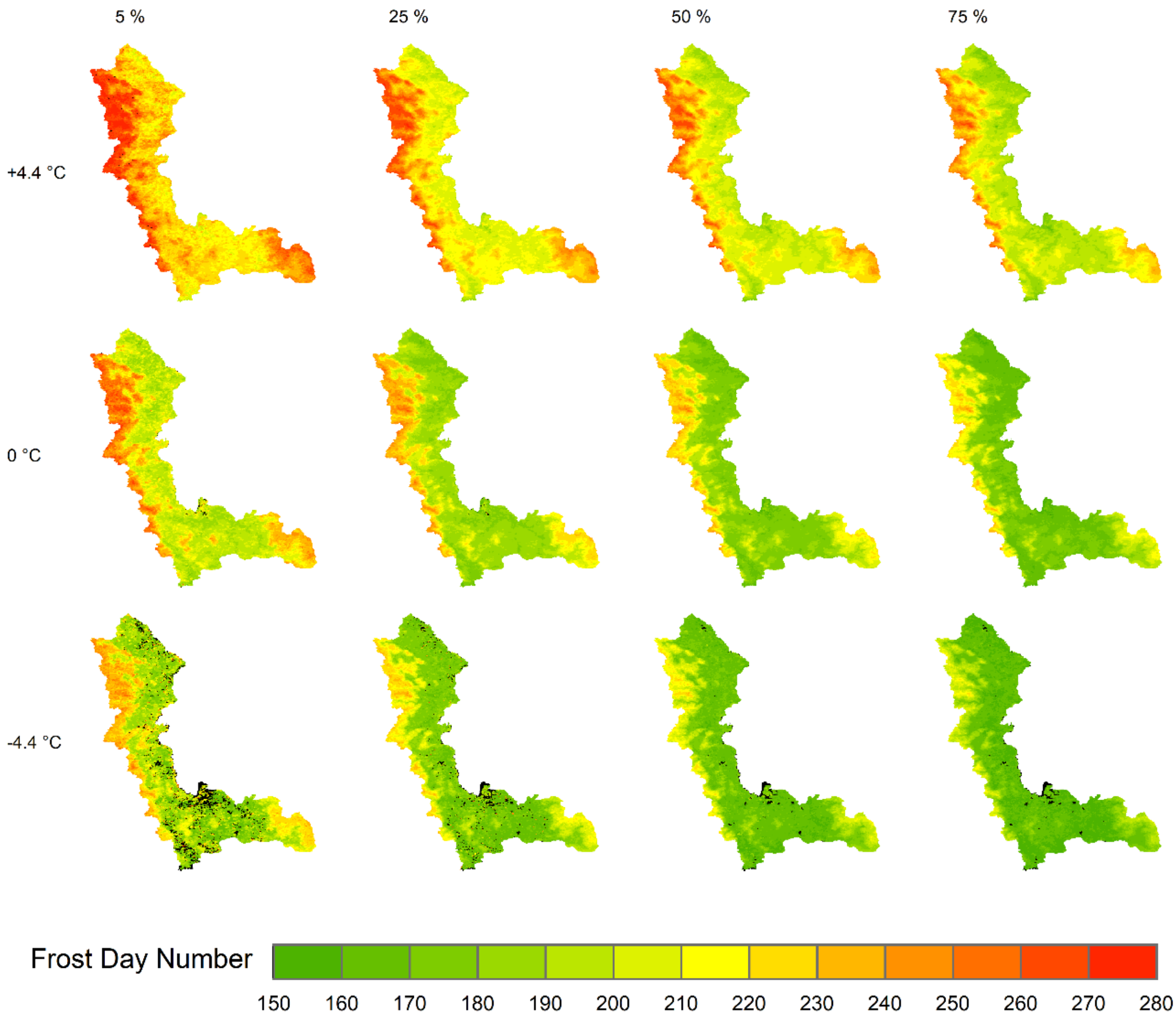

Figure 4. Frost occurrence day number maps for temperature thresholds of +4.4°C, 0°C, and -4.4°C and risks of 5%, 25%, 50%, and 75%.

4. Conclusions

In this study, aimed at analyzing the risk of late spring frosts in West Azerbaijan province, a minimum air temperature estimation model was developed through statistical analysis of daily minimum air temperature data from 20 meteorological stations in West Azerbaijan province, as well as land surface temperature data from satellite remote sensing products and auxiliary data. In the next step, daily minimum temperature maps from this model for the months with the potential for spring frost occurrence in the statistical period of 2000-2023 were used for analyzing late spring frost risk. The achievement of this study is the provision of a code for estimating the risk of frost occurrence for a given day number and a given temperature threshold for frost occurrence, as well as the provision of another code for estimating the day number corresponding to a given risk percentage and a given temperature threshold for frost occurrence. The late spring frost occurrence risk estimation code has the ability to run in 17,690 different states (for different combinations of 145 temperature thresholds in the range of -10°C to +4.4°C with a step of 0.1°C and 122 day numbers from March 1st to June 30th) and can be used as a useful tool for analyzing frost risk for plants with different sensitivities. Also, the frost occurrence day number estimation code has the ability to run in 2,755 different states (for different combinations of 145 temperature thresholds in the range of -10°C to +4.4°C with a step of 0.1°C and 19 risk percentages from 5% to 95% with a step of 5%) and can be used as a useful tool in determining the appropriate planting date for plants so that the sensitive stages of plant growth do not fall within the frost period. The maps obtained from running these codes can be used to determine the appropriate time and place for cultivating crops with different sensitivity thresholds to frost.

The achievements of this study can be used as an important tool for determining the most suitable location and time for cultivating agricultural products in West Azerbaijan province, selecting appropriate frost protection methods in different areas of the province, frost management, and also assisting in hazard assessment and making more accurate decisions by agricultural product insurance funds to estimate frost damage. It is also suggested that the application of the methods used in this study be investigated in the analysis of early autumn frost risk.

References

1. Aghashariatmadari, Z., Bazrafshan, J., Safaei, E. (2016). Projection of the early fall and late spring frosts under climate change condition with SDSM model in several selected stations in the mid-western Iran. Journal of Agricultural Meteorology, 4(1), 22-31.
2. Bazgeer, S., Mohammadi, H., Sharifi, L. and Soleimani, N. (2016). The Analysis of Frost and Chilling Hazards on Horticultural Crops in West Azerbaijan. *Environmental Management Hazards, 3*(4), 365-378.
3. Bazrafshan, J., Rahimi, J. (2014). Radiation, Advection and Mixed Freezing and Frost Risk Assessment and Zoning in Iran. *Journal of Agricultural Meteorology, 2*(1), 67-79.
4. Benali, A., Carvalho, A. C., Nunes, J. P., Carvalhais, N., Santos, A. (2012). Estimating air surface temperature in Portugal using MODIS LST data. Remote Sensing of Environment, 124, 108-121.
5. Falk, R., Miller, N. (1992). A Primer for Soft Modeling. Akron, OH: The University of Akron Press.

Hashemi, F. (1974). Zoning of Iran in terms of agricultural meteorology, Research Publications of the Iranian Meteorological Organization.

6. Hesari, B., Rezaee, R., Nikanfar, R. and Tayefe Neskili, N. (2015). Study and Preparation of Frost Maps for Field and Orchard Crops in West Azarbaijan-Iran. Journal of Geography and Environmental Hazards, 4(2), 117-135.
7. Huschke RE (ed) (1959). Glossary of meteorology. Am Meteorol Soc, Boston, MA, 638 pp.
8. Inouye, D. W. (2000). The ecological and evolutionary significance of frost in the context of climate change. Ecology Letters, 3, 457–463.
9. Janatian, N., Sadeghi, M., Sanaeinejad, S. H., Bakhshian, E., Farid, A., Hasheminia, S. M., Ghazanfari, S. (2017). A statistical framework for estimating air temperature using MODIS land surface temperature data. International Journal of Climatology, 37(3), 1181-1194.
10. Jang, J. D., Viau, A. A., Anctil, F. (2004). Neural network estimation of air temperatures from AVHRR data. International Journal of Remote Sensing, 25(21), 4541–4554.
11. Jin, M., Dickinson, R. E. (2010). Land surface skin temperature climatology: benefitting from the strengths of satellite observations. Environmental Research Letters, 5(4), 44004.
12. Kalma, J.D., Laughlin, G.P., Caprio, J.M., Hamer, P.J.C. (1992). The Occurrence of Frost: Types, Distribution and Prediction. In: The Bioclimatology of Frost. Advances in Bioclimatology, vol 2. Springer, Berlin, Heidelberg.
13. Kalma, J.D., Laughlin, G.P., Green, A.A., O'Brien, M. (1986). Minimum temperature surveys based on near-surface air temperature measurements and airborne thermal scanner data. Journal of Climatology, 6, 413- 430.
14. Kamali, G.H. (2001). Study of the harmful cold weather for Iranian agriculture and preparation of the Iranian Climatic Atlas, Research Publications of Iranian Meteorological Organization.
15. Khalili, A. (2009). Climatic zoning of Iran from the perspective of agricultural product insurance against drought, harmful frosts and torrential rainfall. Applied Research Affairs of the University of Tehran and Agricultural Products Insurance Fund, Volumes 2 and 7.
16. Khalili, A. (2014). Quantitative Evaluation of Spring Frost Risk to Agricultural and Horticultural Crops in Iranand Modeling. Journal of Agricultural Meteorology, 2(1), 17-31.
17. Lamichhane, J. R. (2021). Rising risks of late-spring frosts in a changing climate. Nature Climate Change, 11(7), 554-555.
18. Marino G.P., Kaiser D.P., Gu L., Ricciuto D.M. (2011). Reconstruction of false spring occurrences over the southeastern United States, 1901–2007: an increasing risk of spring freeze damage? Environmental Research Letter, 6, 024015.
19. Mildrexler, D. J., Zhao, M., Running, S. W., Mildrexler, D. J., Zhao, M., Running, S. W. (2011). A global comparison between station air temperatures and MODIS land surface temperatures reveals the cooling role of forests. Journal of Geophysical Research, 116(1), 15.
20. Mostovoy, G. V., King, R. L., Reddy, K. R., Kakani, V. G., Filippova, M. G. (2006). Statistical estimation of daily maximum and minimum air temperatures from MODIS LST data over the state of Mississippi. GIScience and Remote Sensing, 43(1), 78–110.
21. SABKA (2023). Comprehensive Agricultural Insurance System, Agricultural Insurance Fund, Tehran.

22. Vitasse, Y., Rebetez, M. (2018). Unprecedented risk of spring frost damage in Switzerland and Germany in 2017. Climatic Change, 149(2), 233-246.

23. Weiser, C.J., Quamme, H.A., Proebsting, E.L., Burke, M.J., Yelenosky, G. (1979). Plant freeze injury and resistance. In: Barfield BJ, Gerber JF (eds) Modification of the aerial environment of crops. Am Soc Agric Eng Monogr 2. St Joseph, Mich, 55-84.